cyano(2,2'-bipyridyl)nitrosyliron(II) (either trans or cis).

Acknowledgment is made to CONICET (Programa QUINOR), SUBCYT and CICPBA, República Argentina, and BID-FINEP and FAPESP, Brazil, for financial support, to Dr. R. Mercader (FCEUNLP) for running the Mössbauer spectra and for helpful discussions, and to the reviewers for helpful suggestions.

Registry No. $[Fe(bpy)_3][Fe(CN)_5NO]\cdot 4H_2O$, 88245-17-4; $(bpyH)_2[Fe(CN)_5NO]$, 88245-16-3; sodium nitroprusside, 14402-89-2.

Supplementary Material Available: IR spectrum of $[Fe(bpy)_3][Fe(CN)_5NO]\cdot 4H_2O$ in a KBr disk (Figure 3), a stereoscopic ORTEP projection along the crystal unique axis of the asymmetric unit of $[Fe(bpy)_3][Fe(CN)_5NO]\cdot 4H_2O$ (Figure 4), listings of anisotropic thermal parameters for all non-hydrogen atoms (Table V), fractional coordinates of the 2,2'-bipyridyl hydrogens (Table VI), and structure factor amplitudes (Table VII) (16 pages). Ordering information is given on any current masthead page.

Contribution from the Laboratoire de Chimie de Coordination Organique (ERA CNRS 477), Université de Rennes, Campus de Beaulieu, 35042 Rennes Cedex, France, and Laboratoire de Chimie de Coordination du CNRS Associé a l'Université Paul Sabatier, 31400 Toulouse, France

Dehalogenation of Binuclear Arene-Ruthenium Complexes: A New Route to Homonuclear Triruthenium and Heteronuclear Ruthenium-Iron Cluster Complexes Containing Chelating Phosphorus Ligands. Crystal Structure of $Ru_3(CO)_{10}(Ph_2PCH_2PPh_2)$

ANTHONY W. COLEMAN,[†] DENIS F. JONES,[†] PIERRE H. DIXNEUF,*[†] COLETTE BRISSON,[‡] JEAN-JACQUES BONNET,*[‡] and GUY LAVIGNE[‡]

Received February 1, 1983

The binuclear complexes $(RuCl_2(p\text{-cymene}))_2(Ph_2P(CH_2)_nPPh_2)$ (**2**, $n = 2$; **4**, $n = 1$) obtained from $(RuCl_2(p\text{-cymene}))_2$ have been reacted with an excess of $Fe_2(CO)_9$. The former derivative, **2**, yielded $FeRu(CO)_8(Ph_2PCH_2CH_2PPh_2)$ (**5**), $(Fe_2Ru(\mu\text{-}CO)_2(CO)_9)_2(Ph_2PCH_2CH_2PPh_2)$ (**6**), $Ru_3(\mu\text{-}Cl)_2(CO)_8(Ph_2PCH_2CH_2PPh_2)$ (**7**), and $FeRu_2(\mu\text{-}Cl)_2(CO)_8(Ph_2PCH_2CH_2PPh_2)$ (**8**) (noticeably, thermolysis of **8** under mild conditions yielded **7**). The latter derivative, **4**, afforded $Ru_3(CO)_{10}(Ph_2PCH_2PPh_2)$ (**9**) and $FeRu_2(CO)_{10}(Ph_2PCH_2PPh_2)$ (**10**). The X-ray crystal structure of **9** has been determined: monoclinic crystals, space group $P2_1/c$ with $a = 13.122$ (3) Å, $b = 12.040$ (4) Å, $c = 23.658$ (7) Å, $\beta = 103.44$ (2)°, and $Z = 4$. Final R and R_w values are respectively 0.036 and 0.041 on the basis of 4346 independent reflections. The $Ph_2PCH_2PPh_2$ group that bridges a Ru-Ru bond occupies equatorial positions. Interatomic distances of interest are Ru(1)-Ru(2) = 2.834 (1), Ru(1)-Ru(3) = 2.841 (1), and Ru(2)-Ru(3) = 2.860 (1) Å. The shortest bond Ru(1)-Ru(2) is supported by the chelating phosphorus ligand (Ru(1)-P(1) = 2.322 (2) and Ru(2)-P(2) = 2.334 (2) Å). Ru-P bonds are not coplanar as shown by the dihedral angle P(1)-Ru(1)-Ru(2)/P(2)-Ru(2)-Ru(1) = 19.1 (1)°. Such a distortion induces a disturbance in the distribution of CO ligands with respect to $Ru_3(CO)_{12}$. Of particular interest is the bending of every axial carbonyl toward one Ru-Ru bond.

Introduction

Mixed-transition-metal polymetallic complexes have aroused interest recently as much for the novelty of their structure as for the potential offered by their reactivity.[1,2] Among these, ruthenium-iron complexes have specially attracted attention for the versatility of a broad range of phosphine-containing ruthenium catalysts and for the evidence that addition of iron carbonyls to ruthenium catalysts enhances the activity of the catalyst toward the water-gas shift reaction.[3] Moreover, in order to understand how mixed-metal clusters behave as catalysts, or as catalyst precursors, ruthenium-iron complexes have been recently designed for the elucidation of basic reactivity patterns involving a multisite system.[4,5]

In previous work we have indicated that the readily available mononuclear benzene-ruthenium(II) complexes $RuCl_2(PR_3)(C_6H_6)$[6] could act as convenient precursors of $[RuPR_3]$ fragments to afford $FeRu_2(\mu\text{-}Cl)_2(CO)_8(PR_3)_2$ complexes.[7] In the same way, we have now investigated the reactivity of dinuclear arene-ruthenium(II) complexes $(RuCl_2(arene))_2(Ph_2P(CH_2)_nPPh_2)$ toward $Fe_2(CO)_9$ in order to synthesize mixed-metal complexes. We have found that the dehalogenation reaction depends on the nature of the bridging phosphine group, is either partial (with $Ph_2PCH_2CH_2PPh_2$) or complexes (with $Ph_2PCH_2PPh_2$), and affords a series of new mixed-metal iron-ruthenium complexes. Although the use of bimetallic precursors supported by bridging ligands could be expected to provide satisfactory control of the number of Ru centers in the resulting species, we also find trinuclear Ru_3 complexes among the reaction products. Typically, the formation of $Ru_3(CO)_{10}(Ph_2PCH_2PPh_2)$ is an unexpected feature, showing the complexity of the reaction pathway.

The X-ray structure of this complex is reported here. The geometric features are discussed in comparison with those of $Ru_3(CO)_{12}$[8] and $Ru_3(CO)_8(Ph_2PCH_2PPh_2)_2$.[9] The solid-state structure of $Ru_3(CO)_{10}(Ph_2PCH_2PPh_2)$ suggests an alternative mechanism for the previously reported CO-exchange process found for this complex.[10]

[†] Université de Rennes.
[‡] Université Paul Sabatier.

(1) Gladfelter, W. L.; Geoffroy, G. L. *Adv. Organomet. Chem.* **1980**, *18*, 207.
(2) Roberts, D. A.; Geoffroy, G. L. In "Comprehensive Organometallic Chemistry"; Wilkinson, G., Stone, F. G. A., Abel, E. W., Eds.; Pergamon Press: Oxford, 1982; Chapter 40.
(3) Ungermann, C.; Landis, V.; Moya, S. A.; Cohen, H.; Walker, H.; Pearson, R. G.; Rinker, R. G.; Ford, P. C. *J. Am. Chem. Soc.* **1979**, *101*, 5922.
(4) Fox, J. R.; Gladfelter, W. L.; Wood, T. G.; Smegal, J. A.; Foreman, T. K.; Geoffroy, G. L.; Tavanaiepour, I.; Day, V. W.; Day, C. S. *Inorg. Chem.* **1981**, *20*, 3214.
(5) Fox, J. R.; Gladfelter, W. L.; Geoffroy, G. L.; Tavanaiepour, I.; Abdel-Mequid, S.; Day, V. W. *Inorg. Chem.* **1981**, *20*, 3290.
(6) Zelonka, R. A.; Baird, M. C. *Can. J. Chem.* **1972**, *50*, 3063.
(7) Jones, D. F.; Dixneuf, P. H.; Southern, T. G.; Le Marouille, J. Y.; Grandjean, D.; Guênot, P. *Inorg. Chem.* **1981**, *20*, 3247.
(8) Churchill, M. R.; Hollander, F. J.; Hutchinson, J. P. *Inorg. Chem.* **1977**, *16*, 2655.
(9) Lavigne, G.; Lugan, N.; Bonnet, J.-J. *Acta Crystallogr., Sect. B* **1982**, *B38*, 1911.
(10) Cotton, F. A.; Hanson, B. E. *Inorg. Chem.* **1977**, *16*, 3369.

0020-1669/84/1323-0952$01.50/0 © 1984 American Chemical Society

Experimental Section

A. Synthesis. 1. General Comments. All reactions were routinely performed under dry nitrogen atmosphere. Bis(diphenylphosphino)methane (dppm) and bis(diphenylphosphino)ethane (dppe) were purchased from Strem Chemicals. Thick-layer chromatography was performed in the air atmosphere. Layers were made of silica gel 60G (Merck). Positive ^{31}P chemical shifts are downfield from the external H_3PO_4 reference.

2. Preparation of the Complexes. $[RuCl_2(p\text{-}CH_3\text{-}C_6H_4\text{-}CH(CH_3)_2)]_2(Ph_2PCH_2CH_2PPh_2)$ (2). To a suspension of 5 mmol (3.06 g) of $[RuCl_2(p\text{-}CH_3\text{-}C_6H_4\text{-}CH(CH_3)_2]_2$[11] (**1**) in 100 mL of benzene was added 5 mmol (2.0 g) of diphos, and the mixture was refluxed for 4 h. The benzene was removed under vacuum, and the red residue was extracted with chloroform (100 mL). Addition of diethyl ether to the concentrated solution led to the formation of 4 g (80% yield) of red crystals of **2**: ^1H NMR ($CDCl_3$) δ 7.67 (m, C_6H_5), 5.50 (d), 5.27 (d, $p\text{-}C_6H_4$–, $^3J_{HH}$ = 6 Hz), 2.56 (m, CH_2CH_2), 1.90 (s, $CH_3C_6H_4$), 1.00 (d, $(CH_3)_2CH$, $^3J_{HH}$ = 7 Hz); ^{31}P NMR ($CDCl_3$) δ +39.21.

$RuCl_2(p\text{-}CH_3\text{-}C_6H_4\text{-}CH(CH_3)_2)(Ph_2PCH_2PPh_2)$ (3). Five millimoles (3.06 g) of $[RuCl_2(p\text{-cymene})]_2$ (**1**)[11] was reacted with bis(diphenylphosphino)methane (3.84 g, 10 mmol) in 50 mL of dry benzene for 3 h at reflux. After removal of the solvent in vacuo, the red solid residue was extracted with chloroform (75 mL). Addition of diethyl ether to the solution resulted in the formation of 5.2 g of red crystals (75% yield): ^1H NMR ($CDCl_3$) δ 8.10 (m), 7.50 (m), 7.27 (s, C_6H_5), 5.43 (d), 5.30 (d, C_6H_4, $^3J_{HH}$ = 6 Hz), 3.60 (dd, CH_2, $^2J_{PH}$ = 8 and 2 Hz), 2.67 (sept, CH), 2.00 (s, $CH_3C_6H_4$), 0.97 (d, $(CH_3)_2CH$, $^3J_{HH}$ = 7 Hz).

$[RuCl_2(p\text{-}CH_3\text{-}C_6H_4\text{-}CH(CH_3)_2)]_2(Ph_2PCH_2PPh_2)$ (4). Ten millimoles (6.9 g) of **3** and 5 mmol (3.06 g) of $[RuCl_2(p\text{-cymene})]_2$ (**1**)[11] were allowed to react in refluxing benzene (100 mL) for 3 h. The benzene was removed under vacuum, and the red solid was extracted with chloroform (150 mL). The resultant solution was concentrated under vacuum, and orange-red crystals formed by addition of diethyl ether; yield 7.9 g (80%) of **4** obtained by filtration: ^1H NMR ($CDCl_3$) δ 7.70 (m), 7.23 (m, C_6H_5), 5.20 (d), 4.93 (d, $p\text{-}C_6H_4$–, $^3J_{HH}$ = 6 Hz), 4.63 (t, CH_2, $^2J_{PH}$ = 7.5 Hz), 2.53 (sept, CH), 1.92 (s, $CH_3C_6H_4$–), 0.95 (d, $(CH_3)_2CH$, $^3J_{HH}$ = 7 Hz); ^{31}P NMR ($CDCl_3$) δ 38.8.

Reaction of 2 with $Fe_2(CO)_9$. Complex **2** (6 mmol, 6.1 g) and $Fe_2(CO)_9$ (24 mmol, 8.7 g) were refluxed in benzene (80 mL) for 2 h. After filtration and solvent removal, the residue was dissolved in the minimum amount of dichloromethane. Silica gel thick-layer chromatography of the solution (eluent hexane–ether 3:1) showed the presence of many complexes from which were isolated, in order of decreasing migratory capability, **5** (8%, yellow), **6** (10%, violet), **7** (12%, red), and **8** (20%, red). Yields are based on **2**.

$FeRu(CO)_8(Ph_2PCH_2CH_2PPh_2)$ (5): yellow; 0.3 g (8% yield); mp 190–195 °C; IR (Nujol) 2110, 2080, 2050, 1990, 1975, 1965 cm^{-1}. Anal. Calcd for $C_{34}H_{24}O_8P_2FeRu$: C, 52.4; H, 3.1; P, 8.0; Fe, 7.2. Found: C, 53.1; H, 3.2; P, 8.6; Fe, 7.6.

$[(Fe_2Ru(\mu\text{-}CO)_2(CO)_9)]_2(PhPCH_2CH_2PPh_2)$ (6): violet; 0.43 g (10% yield); IR (Nujol) 2110, 2060, 2040, 1990, 1980, 1860, 1820 cm^{-1}; ^1H NMR ($CDCl_6$) δ 7.8–7.3 (m, C_6H_5) (low solubility). Anal. Calcd for $[C_{24}H_{12}O_{11}PFe_2Ru]_2$: C, 40.0; H, 1.7; Fe, 15.5. Found: C, 40.4; H, 1.8; Fe, 15.2.

$Ru_3(\mu\text{-}Cl)_2(CO)_8(Ph_2PCH_2CH_2PPh_2)$ (7): red; 0.72 g (12% yield); mp 150–155 °C (dec); IR (Nujol) 2100, 2040, 2030, 1980, 1935 cm^{-1}; ^{31}P NMR ($CDCl_3$) δ +40.0 (s). Anal. Calcd for $C_{34}H_{24}Cl_2O_8P_2Ru_3$: C, 41.0; H, 2.4; Ru, 30.4; Cl, 7.1. Found: C, 42.2; H, 2.4; Ru, 28.4; Cl, 6.9.

$FeRu_2(\mu\text{-}Cl)_2(CO)_8(Ph_2PCH_2CH_2PPh_2)$ (8): red; 1.14 g (20% yield); mp 175–179 °C (dec); IR (Nujol) 2090, 2060, 2010, 1990, 1970, 1945 cm^{-1}; ^1H NMR ($CDCl_3$) δ 7.8–7.3 (m, C_6H_5), 2.6–2.2 (m, CH_2-CH_2); ^{31}P NMR ($CDCl_3$) δ +43.3. Anal. Calcd for $C_{34}H_{24}Cl_2O_8P_2FeRu_2$: C, 42.9; H, 2.5; Cl, 7.5; P, 6.5; Fe, 5.9; Ru, 21.2. Found: C, 43.2; H, 2.5; Cl, 8.2; P, 6.1; Fe, 5.9; Ru, 20.7.

Reaction of 4 with $Fe_2(CO)_9$. Ten millimoles (9.9 g) of $[RuCl_2(p\text{-cymene})]_2(Ph_2PCH_2PPh_2)$ (**4**) and 40 mmol (14.6 g) of $Fe_2(CO)_9$ were refluxed in benzene (100 mL) for 5 h. After filtration, the benzene was removed under vacuum, and the crude red products were dissolved in dichloromethane and chromatographed on silica gel thick layers (eluent hexane–ether 3:1). From the orange line, which migrated first, 1.5 g (15%) of red crystals of **9** were obtained from hexane–ether solutions. The extraction of the red second line led to the isolation of red crystals (hexane–ether) of **10** (3.5 g, 37% yield).

$Ru_3(CO)_{10}(Ph_2PCH_2PPh_2)$ (9): IR (Nujol) 2100, 2040, 2015, 1990, 1975, 1960, 1950 cm^{-1}; ^1H NMR ($CDCl_3$) δ 7.1–7.6 (m, C_6H_5), 4.3 (t, CH_2, $^2J_{PH}$ = 11 Hz); ^{31}P NMR ($CDCl_3$, 223 K) δ 20.6 (s). Anal. Calcd for $C_{35}H_{22}O_{10}P_2Ru_3$: C, 43.4; H, 2.3; P, 6.4; Ru, 31.3. Found: C, 42.9; H, 2.3; P, 6.0; Ru, 30.3.

$FeRu_2(CO)_{10}(Ph_2PCH_2PPh_2)$ (10): IR (Nujol) 2090, 2040, 2030, 2020, 1990, 1970, 1960, 1910 cm^{-1}; ^1H NMR ($CDCl_3$) δ 7.2–7.6 (m, C_6H_5), 4.2 (t, CH_2, $^2J_{PH}$ = 10.5 Hz); ^{31}P NMR ($CDCl_3$, 309 K) δ +17.2. Anal. Calcd for $C_{35}H_{22}O_{10}P_2FeRu_2$: C, 45.6; H, 2.4; P, 6.7; Fe, 6.0; Ru, 21.9. Found: C, 45.2; H, 2.3; P, 5.9; Fe, 6.1; Ru, 20.5.

B. X-ray Structure Determination of $Ru_3(CO)_{10}(Ph_2PCH_2PPh_2)$ (9). 1. Collection and Reduction of X-ray Data. The crystal selected for X-ray analysis was a red prism bounded by faces $\{\bar{1}11\}$, $\{1\bar{1}\bar{1}\}$, $\{101\}$, $\{\bar{1}0\bar{1}\}$, $\{0\bar{1}2\}$, $\{01\bar{2}\}$. Preliminary photographic data indicated monoclinic symmetry with extinction patterns consistent with the space group $P2_1/c$. Cell constants were obtained from a least-squares fit to the setting angles of 25 reflections ($24° < 2\theta(Mo) < 26°$). These cell constants and other pertinent data are displayed in Table I. A total of 6429 reflections were collected at 21 °C on an Enraf-Nonius CAD4 diffractometer. After processing of the data, using a value of p = 0.03,[12] 4346 unique reflections having $F_o^2 > 3\sigma(F_o^2)$ were used in subsequent calculations.

2. Structure Solution and Refinement. The values of the atomic scattering factors used in the calculations were taken from the usual tabulation[13] including the effects of anomalous dispersion for Ru and P atoms.[14] The hydrogen atom scattering factors were taken from Cromer and Iber's list.[15]

The structure was solved by direct methods.[16] Refinement of an isotropic model including 26 independent atoms and four rigid groups (carbon atoms in phenyl rings were constrained to D_{6h} symmetry; C–C

Table I. Experimental Data for the X-ray Diffraction Study of $Ru_3(CO)_{10}((C_6H_5)_2PCH_2P(C_6H_5)_2)$

fw	956.15
a	13.122 (3) Å
b	12.040 (4) Å
c	23.658 (7) Å
β	103.44 (2)°
V	3635 Å^3
Z	4
d_{calcd}	1.747 g/cm^3
radiation	Mo $K\alpha_1$ = 0.709 30 Å (from oriented graphite monochromator)
linear abs coeff	13.4 cm^{-1}
takeoff angle	4.3°
2θ limits	3.0–48.0°
scan type	ω–2θ
scan speed	2.0°/min
std reflcns	709, 008, 550 (measd every 2 h; no significant deviations)
R	$\Sigma\|\|F_o\| - \|F_c\|\|/\Sigma\|F_o\|$; final value 0.036
R_w	$[\Sigma w^2(\|F_o\| - \|F_c\|)^2/\Sigma w^2\|F_o\|^2)]^{1/2}$; final value 0.041

(11) Bennett, M. A.; Smith, A. K. *J. Chem. Soc., Dalton Trans.* **1974**, 233.

(12) The intensity data were processed as described in: "CAD4 Operation Manual"; Enraf-Nonius: Delft, Holland, 1980. The net intensity is defined as $I = (K/(NPI))(C - 2B)$, where K = 15.44 × (attenuator factor), NPI = ratio of fastest possible scan rate to scan rate for the measurements, C = total count, and B = total background count. The standard deviation in the net intensity is given by $\sigma^2(I) = (K/(NPI)^2)(C + 4B + (pI)^2)$, where p is a factor used to downweight intense reflections. The observed structure factor amplitude F_o is given by $F_o = (I/Lp)^{1/2}$, where Lp = Lorentz and polarization factors. The I's were converted to the estimated errors in the relative structure factors $\sigma(F_o)$ by $\sigma(F_o) = {}^1/_2(\sigma(I)/I)F_o$.

(13) Cromer, D. T.; Waber, J. T. "International Tables for X-ray Crystallography"; Kynoch Press: Birmingham, England, 1974; Vol. IV, Table 2.2A.

(14) Cromer, D. T.; Waber, J. T. Reference 13, Table 2.3.1.

(15) Cromer, D. T.; Ibers, J. A. Reference 13, Table 2.2c.

(16) Besides local programs, modified versions of the following ones were used in solution and refinement of the structure: MULAN, by Germain; FORDAP, the Fourier summation program, by Zalkin; NUCLS, full-matrix least-squares refinement by Ibers; ORFFE, error function program, by Busing and Levy; ORTEP, by Johnson. All calculations were performed on a CII IRIS 80 computer at the Centre Interuniversitaire de Calcul de Toulouse, Toulouse, France.

Table II. Final Positional Parameters with Esd's for $Ru_3(CO)_{10}(Ph_2PCH_2PPh_2)$

atom	x	y	z
Ru(1)	0.17226 (3)	0.07579 (4)	0.34916 (2)
Ru(2)	0.20563 (4)	0.30007 (4)	0.38515 (2)
Ru(3)	0.37814 (4)	0.14872 (5)	0.40224 (2)
P(1)	−0.0022 (1)	0.30001 (4)	0.38515 (2)
P(2)	0.0248 (1)	0.3235 (1)	0.37008 (6)
O(1)	0.2433 (4)	0.0938 (4)	0.2347 (2)
O(2)	0.1124 (3)	0.0621 (4)	0.4671 (2)
O(3)	0.1945 (4)	−0.1748 (4)	0.3460 (2)
O(4)	0.1789 (4)	0.3425 (4)	0.2543 (2)
O(5)	0.2509 (4)	0.2686 (4)	0.5169 (2)
O(6)	0.2920 (5)	0.5328 (5)	0.4130 (3)
O(7)	0.4077 (4)	0.2809 (5)	0.2960 (2)
O(8)	0.3478 (4)	0.0169 (5)	0.5087 (2)
O(9)	0.5565 (5)	0.2742 (6)	0.4817 (3)
O(10)	0.4819 (4)	−0.0541 (6)	0.3628 (3)
C(1)	0.2182 (5)	0.0916 (5)	0.2779 (3)
C(2)	0.1369 (4)	0.0725 (5)	0.4252 (3)
C(3)	0.1853 (5)	−0.0815 (6)	0.3459 (3)
C(4)	0.1896 (5)	0.3203 (5)	0.3016 (3)
C(5)	0.2342 (5)	0.2729 (5)	0.4677 (3)
C(6)	0.2606 (5)	0.4453 (6)	0.4028 (3)
C(7)	0.3891 (5)	0.2351 (7)	0.3342 (3)
C(8)	0.3524 (5)	0.0672 (7)	0.4689 (3)
C(9)	0.4888 (5)	0.2300 (7)	0.4513 (3)
C(10)	0.4442 (5)	0.0218 (7)	0.3782 (3)
C(11)	−0.0465 (4)	0.2440 (5)	0.3061 (2)
H(1)	−0.120	0.244	0.306
H(2)	−0.039	0.283	0.271

Table III. Interatomic Distances (Å) with Esd's for $Ru_3(CO)_{10}((C_6H_5)_2PCH_2P(C_6H_5)_2)$

	A. Ru-Ru		
Ru(1)-Ru(2)	2.834 (1)	Ru(2)-Ru(3)	2.860 (1)
Ru(1)-Ru(3)	2.841 (1)		
	B. Ru-P		
Ru(1)-P(1)	2.322 (2)	Ru(2)-P(2)	2.334 (2)
	C. Ru-C (ax)		
Ru(1)-C(1)	1.928 (6)	Ru(2)-C(5)	1.928 (7)
Ru(1)-C(2)	1.959 (6)	Ru(3)-C(7)	1.949 (8)
Ru(2)-C(4)	1.954 (7)	Ru(3)-C(8)	1.953 (8)
			1.945 [1][a] (av)
	D. Ru-C (eq)		
Ru(1)-C(3)	1.905 (7)	Ru(3)-C(9)	1.905 (8)
Ru(2)-C(6)	1.901 (7)	Ru(3)-C(10)	1.908 (8)
			1.904 [1][a] (av)
	E. C-O (ax)		
C(1)-O(1)	1.144 (7)	C(5)-O(5)	1.136 (6)
C(2)-O(2)	1.119 (6)	C(7)-O(7)	1.134 (8)
C(4)-O(4)	1.127 (7)	C(8)-O(8)	1.131 (8)
			1.131 [3][a] (av)
	F. C-O (eq)		
C(3)-O(3)	1.129 (7)	C(9)-O(9)	1.137 (8)
C(6)-O(6)	1.136 (7)	C(10)-O(10)	1.139 (8)
			1.135 [2][a] (av)

[a] Error estimates shown in brackets for average distances, $\bar{d}$, are the exterior estimates of the precision of the average value given by $[\Sigma_n(\bar{d}-d)^2/(n^2-n)]^{1/2}$.

= 1.394 Å) converged to $R = 0.068$ and $R_w = 0.085$. At this step, hydrogen atoms were introduced and fixed in idealized position (C–H = 0.95 Å); isotropic thermal parameters assigned to hydrogen atoms were taken 1 Å^2 greater than those of their neighbor carbon atoms. Anisotropic thermal parameters were then used for 26 independent atoms. The final full-matrix least-squares refinement, involving 283 variables for 4336 observations, converged to $R = 0.036$ and $R_w = 0.041$. Final atomic coordinates are listed in Table II independent atoms. Selected interatoic distances are in Table III. Bond angles are in Table IV.

Results and Discussion

Synthesis Aspects. The binuclear ruthenium complexes **2** and **4** containing a bis(phosphine) group bridging two identical

Table IV. Interatomic Angles (deg) with Esd's for $Ru_3(CO)_{10}((C_6H_5)_2PCH_2P(C_6H_5)_2)$

	A. Ru_3 Triangle		
Ru(2)-Ru(1)-Ru(3)	60.5 (2)	Ru(1)-Ru(3)-Ru(2)	59.6 (3)
Ru(1)-Ru(2)-Ru(3)	59.8 (2)		
	B. Ru(1) Environment		
C(1)-Ru(1)-Ru(2)	96.4 (2)	C(2)-Ru(1)-P(1)	91.8 (2)
C(1)-Ru(1)-Ru(3)	84.1 (2)	C(2)-Ru(1)-C(3)	93.4 (2)
C(1)-Ru(1)-P(1)	92.1 (2)	C(3)-Ru(1)-Ru(2)	161.8 (2)
C(1)-Ru(1)-C(2)	173.6 (2)	C(3)-Ru(1)-Ru(3)	103.9 (2)
C(1)-Ru(1)-C(3)	90.8 (2)	C(3)-Ru(1)-P(1)	100.9 (2)
C(2)-Ru(1)-Ru(2)	78.2 (2)	P(1)-Ru(1)-Ru(2)	95.5 (1)
C(2)-Ru(1)-Ru(3)	90.2 (2)	P(1)-Ru(1)-Ru(3)	154.9 (1)
	C. Ru(2) Environment		
C(4)-Ru(2)-Ru(1)	80.9 (2)	C(5)-Ru(2)-P(2)	97.3 (2)
C(4)-Ru(2)-Ru(3)	96.8 (2)	C(5)-Ru(2)-C(6)	87.6 (3)
C(4)-Ru(2)-P(2)	87.9 (2)	C(6)-Ru(2)-Ru(1)	165.2 (2)
C(4)-Ru(2)-C(5)	174.4 (3)	C(6)-Ru(2)-Ru(3)	107.9 (2)
C(4)-Ru(2)-C(6)	93.1 (3)	C(6)-Ru(2)-P(2)	104.0 (2)
C(5)-Ru(2)-Ru(1)	97.1 (2)	P(2)-Ru(2)-Ru(1)	89.4 (1)
C(5)-Ru(2)-Ru(3)	77.7 (2)	P(2)-Ru(2)-Ru(3)	147.4 (1)
	D. Ru(3) Environment		
C(7)-Ru(3)-Ru(1)	92.6 (2)	C(8)-Ru(3)-Ru(2)	98.9 (2)
C(7)-Ru(3)-Ru(2)	75.6 (2)	C(9)-Ru(3)-Ru(1)	160.0 (2)
C(7)-Ru(3)-C(8)	174.2 (3)	C(9)-Ru(3)-Ru(2)	103.0 (2)
C(7)-Ru(3)-C(9)	99.1 (3)	C(10)-Ru(3)-Ru(1)	94.1 (2)
C(7)-Ru(3)-C(10)	104.9 (3)	C(10)-Ru(3)-Ru(2)	150.2 (2)
C(8)-Ru(3)-Ru(1)	82.9 (2)		

Scheme I

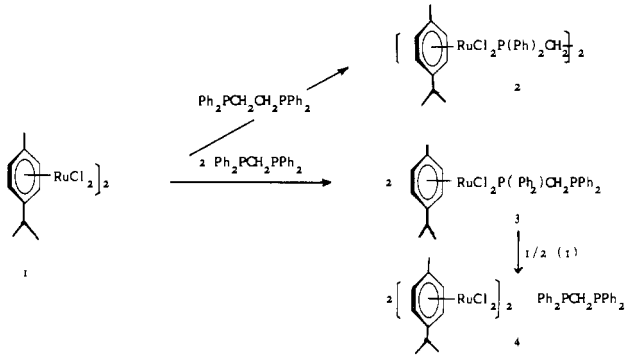

ruthenium(II) centers were obtained easily from $[RuCl_2(p\text{-cymene})]_2$ (**1**)[11] (Scheme I). The addition of 1 equiv of dppe to a benzene solution of **1** led to the isolation of 80% of **2**, according to the previously related addition of monodentate and bidentate ligands to $[RuCl_2(C_6H_6)]_2$.[6,17] In contrast, a pure sample of complex **4** could not be obtained directly and required the isolation of the mononuclear derivative **3**, which was obtained in 75% yield from the addition of dppm to **1**. Subsequent addition of 2 equiv of **3** to a refluxing benzene solution of **1** afforded 80% yield of complex **4**. In both complexes **2** and **4**, the occurrence of a singlet in the ^{31}P NMR is consistent with the equivalence of the two phosphorus atoms (δ ($CDCl_3$): **2**, +39.2; **4**, +38.8).

The potential of both complexes **2** and **4** as precursors for the synthesis of mixed-metal derivatives was examined through the dehalogenation reaction in the presence of $Fe_2(CO)_9$. Complex **2** was first reacted with an excess of $Fe_2(CO)_9$ in refluxing benzene for 2 h. After chromatographic workup, four stable products were isolated (**5**–**8**) and identified as shown in Scheme II. The yellow heterobinuclear complex **5** shows only terminal carbonyls in the infrared spectrum and two nonequivalent ^{31}P nuclei as singlets in ^{31}P NMR (δ ($CDCl_3$): +196.0, +66.3). The violet derivative **6** has an infrared spectrum similar to that of $Fe_2Ru(\mu\text{-}CO)_2(CO)_9(PR_3)$

(17) Faraone, F.; Loprete, G. A.; Tresoldi, G. *Inorg. Chim. Acta* **1979**, *34*, L251.

Scheme II

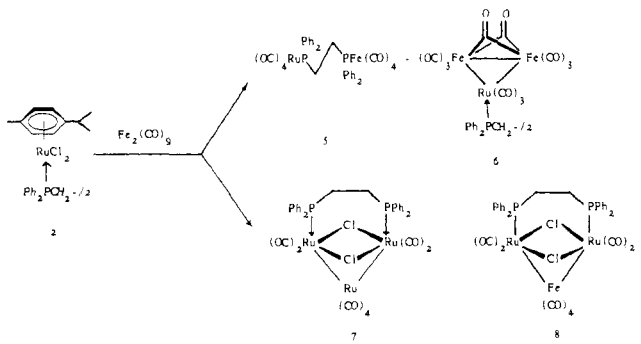

Scheme III

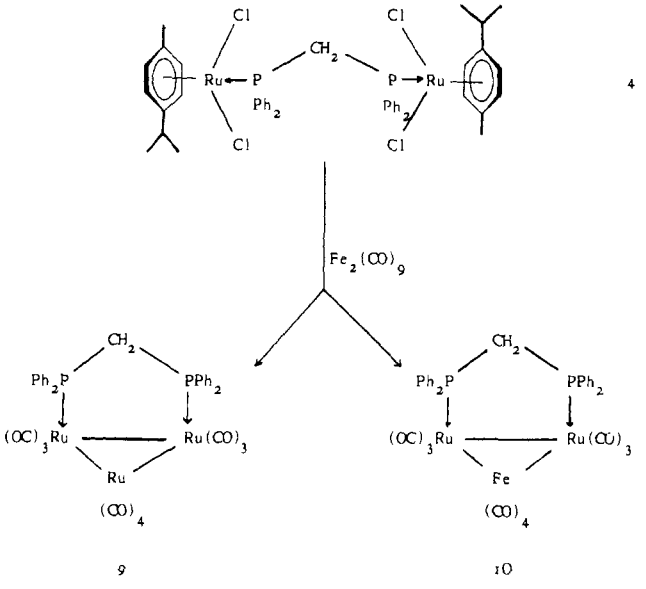

complexes,[7] showing two bands at 1860 and 1820 cm^{-1} corresponding to two carbonyls bridging the iron atoms. As in the dehalogenation reaction of $RuCl_2(PR_3)(C_6H_6)$ by $Fe_2(CO)_9$, the phosphorus group remains linked to the ruthenium atoms.[7] Although significant amount of **7** was obtained in this reaction, we have shown that it could result from a thermolysis of **8**. Similar behavior has been already observed for $FeRu_2(\mu\text{-}Cl_2(CO)_8(PR_3)_2$, yielding $Ru_3(\mu\text{-}Cl)_2(CO)_8(Ph_3)_2$[18] under more drastic conditions than those reported here. The red complex **7** that does not contain any iron, but two chlorines for three Ru atoms, has been formulated as $Ru_3(\mu\text{-}Cl)_2(CO)_8(Ph_2PCH_2CH_2PPh_2)$. The infrared spectrum ressembles that of $Ru_3(\mu\text{-}Cl)_2(CO)_8(PPh_3)_2$[7] and shows only terminal carbonyls. The ^{31}P nuclei are equivalent (δ ($CDCl_3$): +40.0) indicating that the diphos is coordinated to two equivalent Ru atoms, e.g. those bridged by two chloro groups. Finally, the red complex **8** is a $FeRu_2Cl_2P_2$ derivative. A singlet is observed in ^{31}P NMR and the chemical shift (δ $CDCl_3$): +43.3) is similar to that of **7**. These data are consistent with the coordination of the diphos to the Ru atoms bridged by two chloro groups. The known structure of $FeRu_2(CO)_8(\mu\text{-}Cl)_2(Ph_2PC{\equiv}C\text{-}t\text{-}Bu)_2$[7] can be attributed to **8**.

These results show that, apart from the formation of **5** which is typical of **2**, the dppe ligand induces a behavior of the $RuCl_2$(arene)(L) unit which is similar to that induced by PPh_3[7] in that (i) the *p*-cymene ligand is displaced from ruthenium and the vacant sites are occupied by carbonyls and (ii) the partial dehalogenation of ruthenium is favored over complete dehalogenation.

(18) Jones, D. F. These, Université de Rennes, 1981.

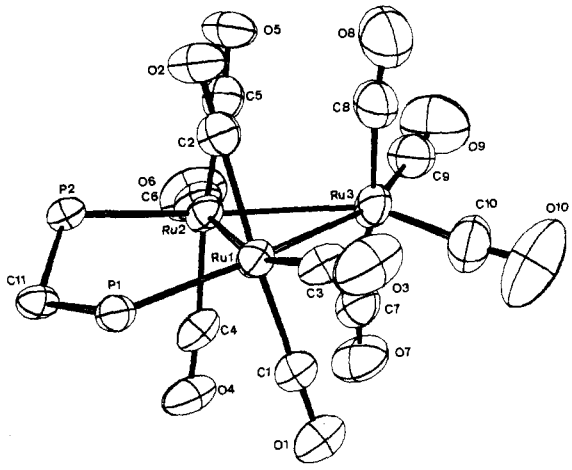

Figure 1. ORTEP diagram of $Ru_3(CO)_{10}(Ph_2PCH_2PPh_2)$. Phenyl rings have been omitted for clarity.

Table V. Selected Dihedral Angles (deg) with Esd's Showing Distortions about Metal Atoms

Ru(1)-Ru(2)-C(2)/Ru(1)-Ru(2)-C(5)	25.7 (2)
Ru(1)-Ru(2)-P(1)/Ru(1)-Ru(2)-P(2)	19.1 (1)
Ru(1)-Ru(2)-C(1)/Ru(1)-Ru(2)-C(4)	23.8 (2)
Ru(1)-Ru(3)-C(2)/Ru(1)-Ru(3)-C(8)	28.4 (3)
Ru(1)-Ru(3)-C(3)/Ru(1)-Ru(3)-C(10)	25.0 (3)
Ru(1)-Ru(3)-C(1)/Ru(1)-Ru(3)-C(7)	29.1 (3)
Ru(2)-Ru(3)-C(6)/Ru(2)-Ru(3)-C(9)	19.8 (3)
Ru(2)-Ru(3)-C(4)/Ru(2)-Ru(3)-C(7)	26.4 (3)
Ru(2)-Ru(3)-C(5)/Ru(2)-Ru(3)-C(8)	29.5 (3)

The reaction of **4** with $Fe_2(CO)_9$ gave by contrast a different result. Treatment of **4** with a large excess of $Fe_2(CO)_9$ in refluxing toluene led to the formation of essentially two red products, **9** and **10** (Scheme III) obtained in 15 and 37% yields, respectively. Both of these complexes do not contain any chlorine and have a structure of the type $M_3(CO)_{10}(Ph_2PCH_2PPh_2)$ with terminal carbonyls. Complex **9** is the trinuclear ruthenium complex that was previously obtained through direct carbonyl substitution of $Ru_3(CO)_{12}$ by $Ph_2PCH_2PPh_2$.[10] Derivative **10** is the homologous heterotrinuclear $FeRu_2$ complex, which is actually the precursor of **9** in this reaction, as shown by its thermolysis in benzene. Both **9** and **10** have equivalent ^{31}P nuclei (δ ($CDCl_3$): **9**, +20.6 (223 K); **10**, +17.2 (309 K)). These data suggest, along with the nature of the precursor **4**, that the dppm ligand is bridging two identical ruthenium atoms in **9** and **10**.

The different behavior of **2** and **4** toward $Fe_2(CO)_9$ indicates that whereas the bridging ligand dppe does not modify significantly the dehalogenation of the $RuCl_2$(arene) units as compared to PPh_3,[7] dppm strongly favors their complete dehalogenation to afford **10** rather than an analogous complex of **8**. Clearly, the use of a bridging ligand maintaining a rather short metal–metal distance, as does the dppm ligand, can favor a metal–metal bond formation required when a complete dehalogenation takes place.

Description and Discussion of the Molecular Structure of $Ru_3(CO)_{10}(Ph_2PCH_2PPh_2)$ (9). A perspective view of the molecular geometry is shown in Figure 1. Selected interatomic distances and angles are given in Tables III and Table IV, respectively, while Table V indicates distortions about metal atoms. As expected from a NMR study,[10] the bridging dppm ligand is coordinated at equatorial sites; it introduces a significant distortion into the trinuclear Ru_3 core as compared with $Ru_3(CO)_{12}$[8] (Ru–Ru range 2.851 (1)–2.859 (1) Å). Among the three Ru–Ru bonds, Ru(1)–Ru(2) supported by the bridging dppm ligand is significantly shorter than unsupported bonds (Ru(1)–Ru(2) = 2.834 (1), Ru(1)–Ru(3) = 2.841 (1), Ru(2)–Ru(3) = 2.860 (1) Å) (Figure 2). A similar

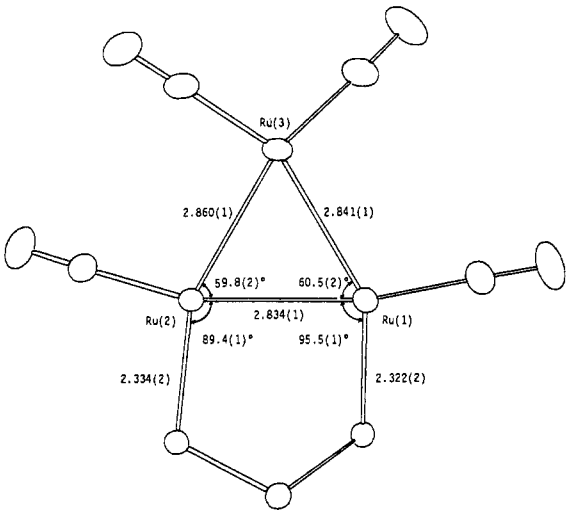

Figure 2. Distribution of equatorial ligands in $Ru_3(CO)_{10}(Ph_2PCH_2PPh_2)$.

shortening influence was previously observed in $Ru_3(CO)_8(dppm)_2$[9] (supported bonds Ru(1)–Ru(2) = 2.826 (2), Ru(1)–Ru(3) = 2.833 (2) Å; unsupported bond Ru(2)–Ru(3) = 2.858 (2) Å). These data contrast with those observed in $Me_2AsC{=}C(AsMe_2)CF_2CF_2$[19] (supported bond 2.858 (3) Å; unsupported bonds 2.831 (3), 2.831 (3) Å). This would seem to indicate that the observed variations in metal–metal bond lengths are related to the strain of the chelated ring, as shown by intracyclic metal–metal–ligand angles. P(1)–Ru(1)–Ru(2) = 95.5 (1)° and P(2)–Ru(2)–Ru(1) = 89.4 (1)° in **9** are small as compared with the corresponding angles in $Me_2As{-}C{=}C(AsMe_2)CF_2CF_2$[19] (As–Ru–Ru = 102.5 (2) and 101.8 (2)°) and in $Ru_3(CO)_{12}$[8] (equatorial OC–Ru–Ru = 98.0 (2)°). Although much more data would be required to rationalize such variations, we suggest that there is some correlation between the mean value for intracyclic Ru–Ru–L angles and the corresponding metal–metal bond distance. The expected trans shortening influence of a phosphorus ligand can be observed in complex **9** since the longest Ru–Ru bond length (Ru(2)–Ru(3) = 2.806 (1) Å) is associated with the longest P–Ru bond length (P(2)–Ru(2) = 2.334 (2), P(1)–Ru(1) = 2.322 (2) Å), which is also the most distorted from the ideal trans position (P(2)–Ru(2)–Ru(3) = 147.4 (1), P(1)–Ru(1)–Ru(3) = 154.9 (1)°) (Figure 2).

Axial ruthenium–carbon bond lengths (average 1.945 (5) Å) are longer than equatorial linkages (average 1.904 (1) Å). Such variations are in full agreement with those previously

(19) Roberts, P. J.; Trotter, J. *J. Chem. Soc. A* **1971**, 1479.

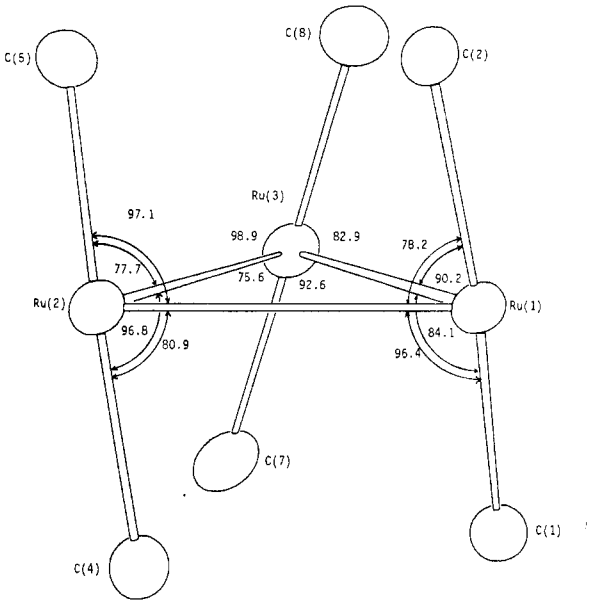

Figure 3. Distribution of axial carbonyls in $Ru_3(CO)_{10}(Ph_2PCH_2PPh_2)$. Angles are given with their esd's of 0.2°.

discussed for $Ru_3(CO)_{12}$.[8] Additional distortions of the CO ligands can be observed in **9**, which can be related to the strain of the chelated ring. The phosphorus atoms are tilted away from the basal plane of the metal triangle; this brings P(1) on one side of the metal triangle and P(2) on the other side (dihedral angle Ru(1)–Ru(2)–P(2)/Ru(2)–Ru(1)–P(1) = 19.1 (1)°). This favored conformation of the chelated ring obviously contributes to the tilting of axial carbonyl ligands away from their precise orthogonal positions. A careful observation of the distribution of these ligands shows that each CO is bent toward only one metal–metal bond, as indicated in Figure 3.

Assuming that the twisted conformation of the chelated ring is retained in solution, the observed distribution of axial carbonyls suggests that the first exchange of carbonyls in complex **9**, which involves only six of the ten carbonyls,[10] may involve the six axial carbonyls. Thus, the first step of the exchange may bridge carbonyls 2 and 4 between Ru(1)–Ru(2), carbonyls 5 and 6 between Ru(2)–Ru(3), carbonyls 1 and 6 between Ru(1)–Ru(3), e.g. the carbonyls that make a short angle (75–87°) with the corresponding Ru–Ru bond (Figure 3).

Registry No. **1**, 52462-29-0; **2**, 88611-19-2; **3**, 88635-40-9; **4**, 88611-20-5; **5**, 88611-21-6; **6**, 88611-22-7; **7**, 88611-23-8; **8**, 88611-24-9; **9**, 64364-79-0; **10**, 88611-25-0.

Supplementary Material Available: Anisotropic thermal parameters (Table S1), rigid-group parameters (Table S2), and observed and calculated structure factors (Table S3) (25 pages). Ordering information is given on any current masthead page.